Positive Delta Detection for Alpha Shape Segmentation of 3D Ultrasound Images of Pathologic Kidneys

Juan J. Cerrolaza[1], Christopher Meyer[1], James Jago[2], Craig Peters[1], and Marius George Linguraru[1,3]

[1] Sheikh Zayed Institute for Pediatric Surgical Innovation, Children´s National Health System, Washington DC, USA
{JCerrola,MLingura}@cnmc.org
[2] Philips Healthcare, Bothell, WA, USA
[3] School of Medicine and Health Sciences, George Washington Univ., Washington, DC, USA

Abstract. Ultrasound is the mainstay of imaging for pediatric hydronephrosis, which appears as the dilation of the renal collecting system. However, its potential as diagnostic tool is limited by the subjective visual interpretation of radiologists. As a result, the severity of hydronephrosis in children is evaluated by invasive and ionizing diuretic renograms. In this paper, we present the first complete framework for the segmentation and quantification of renal structures in 3D ultrasound images, a difficult and barely studied challenge. In particular, we propose a new active contour-based formulation for the segmentation of the renal collecting system, which mimics the propagation of fluid inside the kidney. For this purpose, we introduce a new positive delta detector for ultrasound images that allows to identify the fat of the renal sinus surrounding the dilated collecting system, creating an alpha shape-based patient-specific positional map. Finally, we incorporate a Gabor-based semi-automatic segmentation of the kidney to create the first complete ultrasound-based framework for the quantification of hydronephrosis. The promising results obtained over a dataset of 13 pathological cases (dissimilarity of 2.8 percentage points on the computation of the volumetric hydronephrosis index) demonstrate the potential utility of the new framework for the non-invasive and non-ionizing assessment of hydronephrosis severity among the pediatric population.

Keywords: Collecting system, 3D ultrasound, segmentation, monogenic signal, alpha shapes, kidney, hydronephrosis.

1 Introduction

Thanks to its non-invasive and non-irradiating properties, ultrasound (US) allows quick, safe, and relatively inexpensive evaluation of the kidney and the urinary tract in children. Hydronephrosis (HN), the dilation of the renal collecting system (CS) inside the kidney with distortion of the renal parenchyma caused by the obstruction of the urinary track (see Fig. 1(a)), is one of the most common abnormal finding in these studies, affecting 2-2.5% of children [1] in a wide spectrum of severity. Thus, an early

N. Navab et al. (Eds.): MICCAI 2015, Part III, LNCS 9351, pp. 711–718, 2015.
DOI: 10.1007/978-3-319-24574-4_85

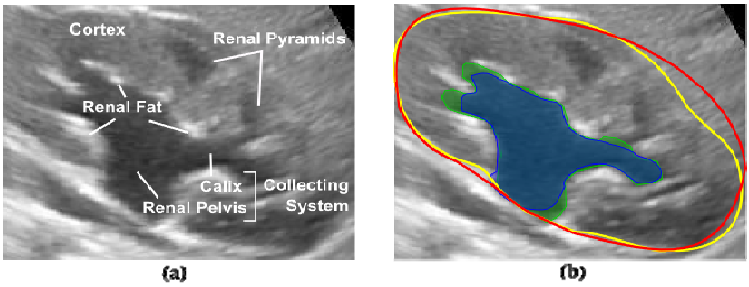

Fig. 1. Renal segmentation in US. (a) US longitudinal view of a hydronephrotic kidney and identification of relevant anatomical structures. (b) Ground truth (GT) and resulting segmentation (RS) for the kidney (GT: yellow; RS: red) and the collecting system (GT: green; RS: blue).

diagnosis is very important in order to identify those cases with severe obstruction of the urinary tract that require immediate surgical intervention. Based on the simple visual inspection of structural abnormalities, the Society for Fetal Urology (SFU) presented a 5-level grading system for classifying and standardizing the severity of HN [2], although its potential as diagnostic tool is limited by the subjective visual interpretation of radiologists. In the assessment of hydronephrosis, it is the effect on kidney function that is of most clincial importance. That assessment has typically been made using radionuclide imaging techniques (i.e., invasive procedures that include exposure to ionizing radiation) to measure relative kidney function and drainage. Though US can only represent the physical structure of the kidney, yet with robust analysis of kidney shape parameters, it has been shown that shape can define clinically relevant functional thresholds to simplify clinical evaluation and reduce the need for invasive imaging. Recently, some works [3,4] have demonstrated the potential value of automated US imaging processing for the quantitative, reproducible, and standardized assessment of HN, with the hydronephrosis index (HI) being one of the most popular methods [3]. HI is computed as $1 - V_{CS}/V_K$, where V_{CS} and V_K represent the volume of the CS and the entire kidney, respectively. In this context, the accurate parameterization and segmentation of the kidney anatomy becomes essential to guarantee an optimal performance and robustness.

Although the quality of US images has increased considerably in recent years, they still suffer from low signal-to-noise ratio, signal attenuation and dropout, and missing boundaries, making the evaluation of organs challenging. Despite the increasing interest in developing new segmentation methods for sonographic images [5] in other application areas like echocardiography, or transrectal ultrasound, there is a dearth of literature discussing the computerized analysis of renal structures. Recently, Cerrolaza et al. [7] proposed a new kidney segmentation framework combining statistical shape models and Gabor-based appearance model tailored to the particularities of the imaging physics of 3DUS. Mendoza et al.[6] presented one of the first approaches to segment both, the kidney and its CS from 2DUS images. However, the segmentation and thus the computation of HI can be significantly affected by the selection of the 2D US slice. To our knowledge, the 3D segmentation of CS remains an unsolved problem. Despite the fact that CS can be partially identified thanks to its hypoechoic nature in hydronephrotic renal US, its segmentation is particularly challenging due to undefined

shape, blurred boundaries, heterogeneous structures of different shapes and intensities inside the kidney (i.e., the renal pyramids in very young children), which can confuse even the experienced eye (see Fig. 1(a)).

In this paper, we present, to the best of our knowledge, the first segmentation and quantification method of the CS in 3DUS. In Section 2.1 we introduce a new positive delta detector for ultrasound images derived from the monogenic signal formulation [9]. This delta detector allows to identify echogenic bands in US images, such as the fat of the renal sinus that surrounds the dilated collecting system. Based on this information, Section 2.2 presents an alpha shape-based patient-specific positional map that controls the evolution of the segmentation process. Section 2.3 presents an original active contour-based formulation, which allows to replicate the evolution of HN in the CS. Finally, the Gabor-based segmentation method for the kidney [7] is incorporated in Section 2.4 to create the complete segmentation framework for renal structures in 3DUS. The segmentation algorithm is tested in Section 3.

2 Methods

2.1 Local Phase-Based 3D Positive Delta Detection

Local phase-based boundary detection methods in US images have been exploited in previous work in the context of echocardiography images [12], showing promising results thanks to reduced sensitivity to speckle and intensity invariance. Given the complex-valued representation of a signal (i.e., the 1D analytic signal based on the Hilbert transform), the local amplitude includes intensity information, whereas the local phase contains local structural information (i.e., location and orientation of image features, such as transitions or discontinuities).

The monogenic signal [9] is a n-dimensional generalization of the 1D analytic representation by means of the Riesz transform. In the context of 3D image processing, the monogenic signal, $\boldsymbol{I}_M$, is defined as the 4D vector $\boldsymbol{I}_M = (\boldsymbol{I}, \boldsymbol{I}_R)$, where $\boldsymbol{I}: \Omega \rightarrow \mathbb{R}^+$ represents the 3D gray level image in the image domain $\Omega \in \mathbb{R}^3$, and $\boldsymbol{I}_R = (\boldsymbol{I}_{Rx}, \boldsymbol{I}_{Ry}, \boldsymbol{I}_{Rz}) = (\boldsymbol{I} * \boldsymbol{h}_x, \boldsymbol{I} * \boldsymbol{h}_y, \boldsymbol{I} * \boldsymbol{h}_z)$ represents the three Riesz filtered components. The spatial representation of the earlier filters is defied by $\boldsymbol{h}_k = -k/(2\pi(x^2 + y^2 + z^2)^{3/2})$, where $k = x, y,$ or z. In practice, the original signal $\boldsymbol{I}$ should be first filtered by an isotropic bandpass filter such as a log-Gabor filter $\boldsymbol{g}_{\boldsymbol{LG},\omega}$, with central frequency ω. Therefore, the monogenic signal can be represented in a polar form by the scalar-valued even component, $even_\omega = \boldsymbol{g}_{\boldsymbol{LG},\omega} * \boldsymbol{I}$, and odd component, $odd_\omega = (\sum_{k=x,y,z}(\boldsymbol{g}_{\boldsymbol{LG},\omega} * \boldsymbol{I}_{Rk})^2)^{1/2}$. Using this representation of the monogenic signal, the local phase [13] can be defined as $\Phi_\omega = \operatorname{atan}(even_\omega / odd_\omega)$, with $\operatorname{atan}(.)$ being the inverse tangent in radians. Typically, the properties of the local phase are used to detect step edges in images identifying those points whose absolute value of the local phase is 0 (positive edges), or π (negative edges) [13]. However, local phase properties can also be exploited to detect symmetrical image features such as positive (ridge) or negative (valleys) deltas, identified with points whose local phase is $+\pi/2$, or $-\pi/2$, respectively. In particular,

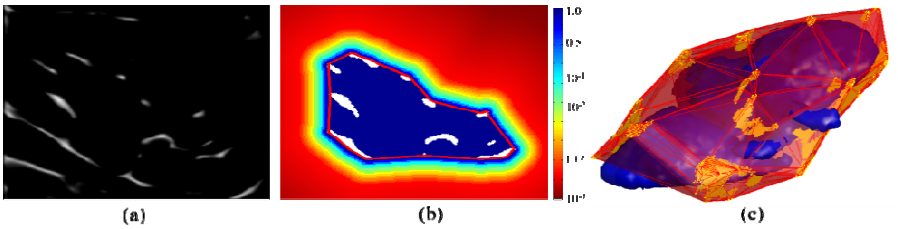

Fig. 2. Renal patient specific positional map. (a) Example of 3D positive delta detection for the US image shown in Fig. 1(a). (b) Alpha shape (red contour) and resulting positional map from the fat points inside the segmented kidney shown in Fig. 1(a). (c) 3D alpha shape (red) surrounding the collecting system (blue). The detected fat points are shown in yellow.

we are interested in relatively thin echogenic regions (i.e., ridges) inside the kidney, corresponding to fat tissue, originally located in the renal sinus and displaced towards the interior of the kidney due to the dilation of the CS in hydronephrotic cases. These bands of fat surround the dilated CS and constitute a key visual clue for the radiologist to differentiate the CS from other hypoechoic structures like the renal pyramids (see Fig. 1(a)). Inspired by the phase congruency theory proposed by Kovesi [13], we propose a multi-scale positive delta detector (PDD) identifying those regions where the local phase is $+\pi/2$, i.e., points where $|even_\omega| \gg |odd_\omega|$ and $sign(even_\omega \cdot odd_\omega) > 0$. Since positive deltas, like step edges, are scale-dependent features, the multiple-scales PDD is defined as

$$\mathrm{PDD} = \sum_\omega \frac{\lfloor |even_\omega| - |odd_\omega| - T_\omega \rfloor \cdot sign(even_\omega \cdot odd_\omega)}{\sqrt{odd_\omega{}^2 + even_\omega{}^2 + \varepsilon}}, \quad (1)$$

where the $\lfloor \cdot \rfloor$ operator zeros the negative values, ε is a small positive constant to prevent division by zero, and T_ω is a scale specific noise threshold defined as $T_\omega = \exp(mean[\log((odd_\omega{}^2 + even_\omega{}^2)^{1/2})])$. In particular, PDD $\in [0,1]$, taking values close to 1 near bright bands (i.e., positive delta features), and close to zero otherwise (see Fig. 2(a)).

2.2 Patient Specific Positional Maps via Alpha Shapes

Having identified the fat areas inside the kidney, the goal is to create an anatomically-justified stopping criteria for the active contour formulation that prevents the leak of the contour outside the region delimited by the fat tissue. However, most of the existing surface reconstruction techniques from point sets (i.e., fat points located via PDD) assume a densely-sampled point cloud, which is not the case in most of hydronephrotic kidneys, where the scattered distribution of the inner thin fat results in an unstructured set of dispersed points. Here, we describe this region as the 3D alpha shape [14], S_α, defined by the fat points identified by PDD (see Fig.2(c)). Alpha shapes are a generalization of the concept of convex hull that allow to recover the shape of non-convex and even non-connected sets of points in 3D. In our case, alpha shapes provide an elegant and efficient solution to the problem of estimating the

intuitive notion of the shape defined by the fat regions. In particular, the level of detail of the polyhedron is controlled by the single configuration parameter, $\alpha \in \mathbb{R}^+$, with S_∞ being equivalent to the convex hull defined by the points. Thus, the new stopping function can be defined as $\mathrm{SF}(\mathbf{x}) = 1/(1 + \left|D_{S_\alpha}(\mathbf{x})\right|)^\tau$, where $\mathbf{x} \in \Omega$ defines a point in the image domain, $D_{S_\alpha}(\mathbf{x})$ is the signed distance to S_α, taking negative or positive values inside and outside S_α, respectively, and $\tau \in [1, +\infty)$ is a control variable (see Fig. 2(b) and (c)). Note that the computation of $\mathrm{SF}(.)$ can be performed offline for the entire image domain, Ω, since it does not depend on the evolution of the contour. This new stopping function is integrated in the active contour evolution equation in the next section.

2.3 Active Contours Formulation

To address the segmentation of the CS, we employ an active contour approach [8]. In particular, we propose a new energy functional that combines contour and intensity-based terms, incorporating the patient-specific positional map described above as additional stopping criteria.

Suppose $\boldsymbol{I}: \Omega \to \mathbb{R}^+$ represents a 3D gray level image in the image domain $\Omega \in \mathbb{R}^3$, and $\boldsymbol{U}: (t, \Omega) \to \mathbb{R}$ is an implicit representation of the surface $\boldsymbol{S}$, which coincides with the set of points $\boldsymbol{U}(t, .) = 0$. Following the geodesic active contours formulation proposed by Caselles et al. [8], the evolution of $\boldsymbol{U}$ is defined by $\boldsymbol{/\partial t} = g(\boldsymbol{I})|\nabla \boldsymbol{U}|(\kappa + c) + \nabla g(\boldsymbol{I}) \cdot \nabla \boldsymbol{U}$, where $\kappa = div(\nabla \boldsymbol{U}/|\nabla \boldsymbol{U}|)$ is the curvature term computed on the level set of $\boldsymbol{U}$, $c \in \mathbb{R}^+$ is a constant velocity term, and $g(\boldsymbol{I})$ is an inverse edge indicator function of the image $\boldsymbol{I}$. The constant expanding force represented by c prevents the contour to get stuck at local minimum when dealing with noisy and low contrast data in US images. Additionally, the constant expanding force represented by c can be interpreted as the expansive dilation force that pushes the dilation of CS inside the kidney. The directionality of the expansion process of the CS (i.e. the dilation of the CS is not uniform in space; see Fig. 1(a)) is controlled by the patient specific positional map described in Section 2.2. Typically, $g(\boldsymbol{I})$ is defined as $g(\boldsymbol{I}) = 1/(1 + |\nabla(G_\sigma * \boldsymbol{I})|)$, with G_σ representing a Gaussian kernel with standard deviation σ. However, this typical intensity-based method of boundary detection generally performs poorly in US due to the aforementioned drawbacks. As alternative, we use the feature asymmetry detector (FA) [13] (i.e., a local phase-based step function detector) whose satisfactory performance as edge detector in US images was emphasized by previous works [10,12]. Thus, the inverse edge indicator function can be defined as $(\boldsymbol{I}) = 1 - FA^\gamma$, with $\gamma \in [0,1]$.

The terms described above are all expansive forces controlled by the external image dependent stopping function, $g(\boldsymbol{I})$, whose main goal is to stop the evolving surface when it arrives to the object boundaries. However, it turns inefficient when segmenting objects with weak or missing boundaries. Here we combine the above gradient-based active contour model with the minimal variance formulation proposed by Chan and Vese [11], whose more general formulation defines the evolution of the contour as $\partial \boldsymbol{U}/t = (\lambda_{out}(\boldsymbol{I} - \mu_{out})^2 - \lambda_{in}(\boldsymbol{I} - \mu_{in})^2)|\nabla \boldsymbol{U}|$, where μ_{out}, and μ_{in} are the mean intensities in the exterior and the interior of the surface $\boldsymbol{S}$, respectively; λ_{out}

and λ_{in} are two control parameters generally defined as $\lambda_{out} = \lambda_{in} = 1$. With this formulation, the segmentation turns into an optimization process that looks for the best separating contour in $\boldsymbol{I}$, and the optimal expected values μ_{out} and μ_{in}. Given the hypoechoic nature of the CS in US images (i.e., $\mu_{in} \approx 0$), the second term of the above equation prevents the evolution of the contour into brighter areas, whereas the first term acts as expansive force toward dark areas (i.e., toward the CS). Finally, incorporating the alpha shape-based patient-specific positional map as additionally stopping function, the final evolution equation of the active contour is defined as

$$\frac{\partial \boldsymbol{U}}{\partial t} = \mathrm{SF}(\boldsymbol{I})\Big(\beta\big((\kappa + c)g(\boldsymbol{I})|\nabla \boldsymbol{U}| + \nabla \mathrm{g}(\boldsymbol{I}) \cdot \nabla \boldsymbol{U}\big) + (1-\beta)\big((\lambda_o(\boldsymbol{I}-\mu_o)^2 - \lambda_i(\boldsymbol{I}-\mu_i)^2)|\nabla \boldsymbol{U}|\big)\Big), \quad (2)$$

where $\beta \in \mathbb{R}^+$is a constant that balances the contour- and the intensity-based terms.

2.4 Complete Segmentation Framework of Renal Structures in 3DUS

The kidney (including CS) Gabor-based segmentation method recently proposed by Cerrolaza et al. [7] is now integrated with the CS segmentation approach described above, creating a complete framework for the segmentation and quantification of hydronephrosis in 3DUS. The semi-automatic algorithm proposed in [7] requires minimal user intervention, selecting two point clicks to roughly define the major axis of the kidney. Within the segmented kidney, the segmentation of CS is automatically initialized by selecting the darkest $3 \times 3 \times 3$ region within S_α. Using the initial segmentation of the kidney to filter those spurious adipose points outside the renal tissue, an estimation of S_α is obtained and the CS is segmented. Finally, the volumetric HI is automatically computed as explained in Section 1.

3 Results and Discussion

To validate the new framework for the analysis of renal structures, we used a set of 13 3DUS image of pathologic pediatric right kidneys diagnosed with hydronephrosis of varying severity. Image data were acquired from a Philips iU22 system with X6-1 xMATRIX Array transducer. The average image size was $484 \times 404 \times 256$ voxels, with a resolution range from 0.15 mm to 0.82 mm. For each image, the kidney and CS were delineated manually by an expert radiologist to provide the ground truth. The method was evaluated using the leave-one-out cross-validation. The statistical shape model used in the kidney segmentation method was refined using an additional set of 11 healthy kidney cases. The same configuration parameters described in [9] were used during the experiments. The rest of the configuration parameters were determined empirically using an iterated grid search approach. In particular, the selected values were: $c = 1$, $\lambda_{out} = \lambda_{in} = 1$, $\beta = 0.3$, $\alpha = 60$, and $\tau = 9$. For the local phase-based feature detection, we use a bank of log-Gabor filters with central frequencies $\omega = 0.04, 0.05$ and 0.06. Two point clicks were manually defined to initialize the segmentation of the kidney, while the CS was initialized automatically, as described in Section 2.4 A valid initialization seed (i.e., a $3 \times 3 \times 3$ region inside the CS) was automatically detected in 11 cases; in the other two images, the location of

the seed was corrected manually. No significant difference was observed for different initializations, provided that the seed is located inside the CS.

Table 1 shows the segmentation error of both the kidney and CS. Although the method proposed here is the first segmentation framework for the CS in 3DUS, the performance of this new approach is compared with our 3D version of the graph cut-based method described by Mendoza et al. [8], originally conceived for 2DUS. It can be observed how the new framework provides not only better average results, but also lower standard deviation for the two accuracy metrics considered: Dice's coefficient (DC), and symmetric point-to-surface distance (SPSD). This improvement was statistically significant (p-value < 0.05 for both metrics), as assessed by means of a Wilcoxon paired signed non-parametric test. In particular, the new method provides an average DC of 0.75 ± 0.08, similar to the inter-user accuracy reported by [6], 0.76 ± 0.18 (p-value > 0.2 using a two-sample t-test between the mean values).

Table 1. Segmentation accuracy evaluation of the kidney and the CS segmentation using the new tailored active contour-based approach (CS-TAC), and the graph cut-based method proposed in [6] (CS-GC). The table present the average error and standard deviation for the Dice's coefficient (DC), and the symmetric point-to-surface distance (SPSD).

	Kidney		CS-TAC		CS-GC	
	MEAN	STD	MEAN	STD	MEAN	STD
DC	0.80	0.06	0.75	0.08	0.62	0.19
SPSD(mm)	2.30	0.80	0.98	0.27	1.35	1.20

Finally, the potential utility of the new segmentation framework for the assessment of pediatric hydronephrosis was evaluated computing the volumetric HI for all the cases (computed as percentage). The average error provided by the full semi-automatic framework detailed in Section 2.3 was 2.8 ± 3.30 percentage points. Compared to the subjective and commonly used SFU grading system, 3DHI provides a quantitative measurement for hydronephrosis severity, allowing objective longitudinal monitoring of the patient by US. The ability to objectively assess kidneys with hydronephrosis without using invasive imaging with ionizing radiation would be of great clinical value. This would permit establishment of thresholds where less complex imaging would be safe and effective for ongoing monitoring and assessment.

A Matlab® implementation of the framework was tested on a 64-bit 2.8 GHz processor, with an average execution time of 321 s (kidney: 96 s and CS: 225 s), which represents a considerable improvement over the several hours it takes for the unreproducible manual delineation by an operator.

4 Conclusions

In this paper, we present the first complete framework for the segmentation and quantification of renal structures in 3DUS. Thanks to the new positive delta detector introduced here, bands of fat inside the kidney are successfully identified, allowing us to define positional maps of the dilated collecting system via alpha shapes-based volume

reconstruction. This patient-specific information is integrated into a hybrid contour-based formulation for the segmentation of the collecting system, combining contour- and intensity-based propagation terms. Finally, a Gabor-based semi-automatic segmentation of the kidney is incorporated to create the first complete ultrasound-based framework for the quantification of hydronephrosis. The promising results obtained in the segmentation and the estimation of the volumetric hydronephrosis index demonstrate the potential utility of the new proposed framework for the assessment of hydronephrosis among the pediatric population using non-invasive non-ionizing US images. In particular, the system provides objective and accurate information of the renal parenchymal status, which allows for better informed clinical decision making.

References

1. Peters, C., Chevalier, R.: Congenital Urinary Obstruction: Pathophysiology and Clinical Evaluation. In: Wein, A., Kavoussi, L., Novick, A., Partin, A., Peters, C. (eds.) Campbell-Walsh Textbook of Urology, vol. 4, pp. 3028–3047. Elsevier, Inc, Philadelphia
2. Fernbach, S.K., et al.: Ultrasound Grading of Hydronephrosis: Introduction to the System Used by the Society for Fetal Urology. Pediatric Radiology 23(6), 478–480
3. Shapiro, S., et al.: Hydronephrosis Index: A New Method to Track Patients with Hydronephrosis Quantitatively. Urology 72(3), 536–538 (2008)
4. Cerrolaza, J.J., et al.: Ultrasound Based Computer-Aided-Diagnosis of Kidneys for Pediatric Hydronephrosis. SPIE Medical Imaging, paper 9035-102 (2014)
5. Noble, J.A., et al.: Ultrasound image segmentation: a survey. IEEE Trans. on Med. Imag. 25(8), 987–1009 (2006)
6. Mendoza, C.S., et al.: Automatic Analysis of Pediatric Renal Ultrasound Using Shape, Anatomical and Image Acquisition Priors. In: Mori, K., Sakuma, I., Sato, Y., Barillot, C., Navab, N. (eds.) MICCAI 2013, Part I. LNCS, vol. 8151, pp. 259–266. Springer, Heidelberg (2013)
7. Cerrolaza, J.J., et al.: Segmentation of Kidney in 3D-Ultrasound Images Using Gabor-based Appearance Models. In: IEEE Int. Symp. on Biom. Imag., 633–636 (2014)
8. Caselles, V., et al.: Geodesic Active Contours. Int. Journal of Comp. Vis. 22(1), 61–79 (1997)
9. Felsberg, M., Sommer, G.: The Monogenic Signal. IEEE Trans. on Sig. Proc. 49(12), 3136–3144 (2001)
10. Belaid, A., et al.: Phase-Based Level Set Segmentation of Ultrasound Images. IEEE. Trans. on Inf. Tech. in Biomed. 15(1), 138–147 (2011)
11. Chan, T.F., Vese, L.A.: Active Contours Without Edges. IEEE Trans. Image Proc. 10(2), 266–277 (2001)
12. Rajpoot, K., et al.: Local-Pase Based 3D Boundary Detection Using Monogenic Signal and its Application to Real-Time 3-D Echocardiography Images. IEEE ISBI (2009)
13. Kovesi, P.: Image Features from Phase Congruency. J. Comput. Vis. Res. 1(3), 1–26 (1999)
14. Edelsbrunner, H., et al.: On the Shape of a Set of Points in the Plane. IEEE Trans. Inf. Theory 29(4), 551–559 (1983)